



The impact of vibrational spectroscopy with neutrons on our view of quantum dynamics in hydrogen bonds and proton transfer

F. Fillaux*

LADIR-CNRS, UMR 7075 Université Pierre et Marie Curie, Groupe des Laboratoires de Vitry-Thiais, 2, rue Henri Dunant, 94320 Thiais Cedex, France

Received 12 October 2001; revised 10 December 2001; accepted 21 December 2001

Abstract

The inelastic neutron scattering technique (INS) reveals new aspects of the proton dynamics in hydrogen bonds, which could not be observed with the infrared and Raman techniques. We briefly review the main advantages of this technique and we present a few examples of new proton dynamics recently observed. In KHCO_3 , the proton dynamics are largely decoupled from the lattice and cannot be represented with usual ‘molecular’ force fields. The double minimum potentials for the transfer of a single proton along the hydrogen bond for KHCO_3 and benzoic acid are compared. In both case, the $0 \rightarrow 1$ transition is clearly observed with INS. The potential barriers of $\sim 5000 \text{ cm}^{-1}$ are very similar. Consequently, the transfer occurs exclusively via tunnelling and semi-classical jumps over the barrier can be ignored. The infrared spectrum of an isotopic mixture demonstrates that proton transfer dynamics in the centrosymmetric dimers are uncorrelated. In addition, proton transfer occurs without any visible rearrangement of the carboxylic group structure and the effective proton mass is close to 1 amu. © 2002 Elsevier Science B.V. All rights reserved.

Keywords: Inelastic neutron scattering; Vibrational spectroscopy; Hydrogen bonding; Proton transfer; Tunnelling

1. Introduction

Proton transfer along hydrogen bonds is of fundamental importance to many physical, chemical and biochemical processes [1–10]. There is a general agreement that proton transfer dynamics have properties characteristic of a light particle in a heavy framework that can be represented with an effective potential along a local reaction coordinate coupled to the motions of heavy atoms [11–40]. In simple linear systems such as $\text{XH}\cdots\text{Y}$ the potential energy for the hydrogen atom along the hydrogen bond may have

two inequivalent minima corresponding to the schematic structures $\text{XH}\cdots\text{Y}$ and $\text{X}^-\cdots\text{H}^+\text{Y}$, respectively. The top of the potential barrier corresponds to the transition-state. Only in symmetric systems $\text{AH}\cdots\text{A}$, the two wells can be equivalent and proton transfer mediated by ‘tunnelling’ may take place, even at very low temperature. Indeed, there is a manifold of intermediate cases between perfectly symmetric and highly asymmetric systems. In all cases, the key parameters for proton transfer dynamics are the distance between the two wells (R), the barrier height (E_a), the potential asymmetry (ΔU) and the tunnelling matrix element (ν_{0t}). In addition, proton transfer occurs in a complex multidimensional environment and strong coupling with the surrounding degrees

* Tel.: +33-1-49-781283; fax: +33-1-49-781118.
E-mail address: fillaux@glvt-cnrs.fr (F. Fillaux).

of freedom is also regarded as a major factor determining the transfer rate. According to the great complexity of the microscopic mechanism for proton transfer an accurate determination of these parameters from experimental and theoretical studies is not easy.

From the theoretical viewpoint, there is no unique way to partition the binding energy resulting from simultaneous changes of the electronic and vibrational wave functions upon hydrogen bond formation [8]. Modelling of proton transfer dynamics with quantum chemistry is further hampered by the complexity of treating thermal and quantum fluctuations in complex systems with high accuracy [9,41–43]. On the other hand, the characterisation of hydrogen bonds and proton transfer with experimental means is often ambiguous as each particular approach highlights a different view. Structural studies emphasise bond lengths and angles [44,45]. NMR and quasi-elastic neutron scattering (QENS) are mainly concerned with dynamics at a rather long time-scale (typically longer than $\sim 10^{-10}$ s) [11–31,46] whilst quantum effects are observed with vibrational spectroscopy [47,48]. Consequently, quite different views of the proton transfer mechanism have emerged from previous works.

2. The impact of inelastic neutron scattering

Protons dynamics in the quantum regime are best observed with the vibrational spectroscopy techniques on a time-scale shorter than 10^{-10} s. The infrared and Raman techniques suffer from limitations due to the nature of interaction of photons with matter. Most of these limitations are irrelevant if neutrons instead of photons are used to perform incoherent inelastic neutron scattering (INS) experiments.

For optical techniques, intensities are related to the derivatives of either the dipole moment in the infrared, or the polarizability tensor in Raman. These quantities are very sensitive to the hybridisation state of valence electrons. They are largely unknown, as they cannot be measured directly and quantum calculations are not yet able to provide reliable values. Therefore, measured intensities cannot be fully exploited. With INS, the neutron scattering process is entirely attributable to nuclear interactions and cross-sections are independent of chemical bonding.

Transition moments can be calculated accurately and compared to measured intensities. In addition, there is no symmetry related selection rule.

Because the proton cross-section for incoherent neutron scattering is one order of magnitude greater than that for any other atom, proton dynamics can be studied in many different non-hydrogenous environments. This proton selectivity can be further exploited because the deuterium atom has a very much smaller cross-section than the proton. For a system with several protons, specific deuteration of some sites therefore simplifies the observed signals. As a result, INS intensities provide information on proton dynamics that can be analysed with greater confidence than the corresponding infrared and Raman spectra.

The INS spectroscopy offers a unique opportunity to measure vibrational spectra over a broad range of energy and momentum transfer ($\mathbf{Q} = \mathbf{k}_i - \mathbf{k}_f$ with wave-vector amplitudes $|\mathbf{k}_i| = 2\pi/\lambda_i$ and $|\mathbf{k}_f| = 2\pi/\lambda_f$, where λ_i and λ_f are the incident and scattered wavelengths, respectively). The intensity for incoherent scattering by protons can be represented with the scattering function [49]

$$S(\mathbf{Q}, \omega) = |\langle \Psi_f(\mathbf{r}) | \exp(i\mathbf{Q}\cdot\mathbf{r}) | \Psi_i(\mathbf{r}) \rangle|^2 \delta(E_{if} - \hbar\omega). \quad (1)$$

$\Psi_i(\mathbf{r})$ and $\Psi_f(\mathbf{r})$ are the wave functions, in the initial and final states, respectively. They depend on the spatial coordinate \mathbf{r} . E_{if} is the energy of the transition and $\hbar\omega$ is the neutron energy transfer. For each vibrational mode, the INS spectral profile in \mathbf{Q} contains spatial information on the wave functions. For optical techniques $\mathbf{Q} \approx 0$.

In many materials, photons are strongly absorbed or refracted over wide frequency ranges. Only the extremely thin layer at the surface can be observed. In contrast to this, neutrons can penetrate most media and probe proton dynamics in the bulk.

Vibrational spectroscopy with neutrons already has achieved results of interest across most of the classic disciplines of physics, chemistry and biology. INS appears more and more complementary to optical techniques. New results obtained with INS allow us for a better understanding of infrared and Raman and consequently a more effective use of these techniques.

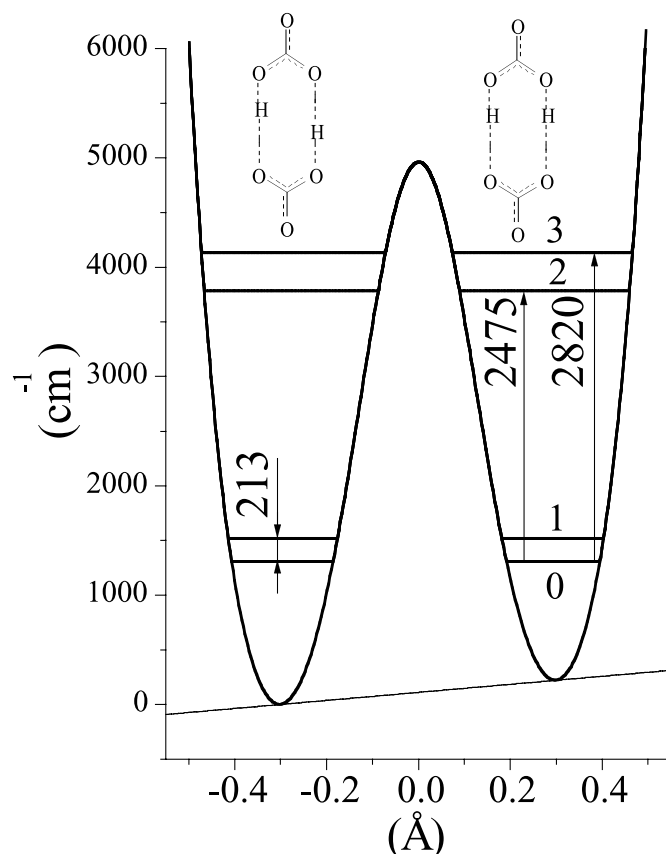


Fig. 1. Potential function for the proton-stretching mode in KHCO_3 , after Ref. [62,71]. The two minima are at $\pm 0.3 \text{ \AA}$ and the barrier height is $\sim 5000 \text{ cm}^{-1}$.

2.1. Force fields calculations: normal versus localised modes

It is widely accepted that vibrational dynamics of atoms and molecules are reasonably well represented with harmonic force fields. The resolution of the secular equation transforms a set of (say N) coupled oscillator into (N) independent oscillators along orthogonal (normal) coordinates. Eigenvalues of the dynamical matrix are normal frequencies and eigenvectors give atomic displacements for each normal mode [50–55]. If band intensities cannot be fully exploited, these vectors are unknown and force fields refined with respect to observed frequencies only are largely undetermined. For complex systems, symmetry consideration or/and isotopic substitutions may remove only partially this under determination.

With the INS technique, force fields can be refined with respect to the full spectral profiles including both frequencies and intensities [56–61]. This technique is most powerful for hydrogenous samples for which intensities are dominated by modes involving large proton displacements. However, contributions from other atoms are difficult to estimate precisely and can be easily overlooked.

When harmonic force fields are used to represent local atom–atom interactions in molecular crystals, the mean positions of the protons oscillating at high frequency (internal modes) follow adiabatically the slow lattice vibrations. This proton riding effect should give rise to large intensities for lattice modes at low frequency. Moreover, intensities for internal molecular vibrations should be depressed dramatically by an exponential term referred to as the

Debye–Waller factor, $\exp[-\langle(\mathbf{Q}\cdot\mathbf{u})^2\rangle]$, where \mathbf{u} is the displacement vector for atoms and $\langle\rangle$ means ‘averaged over the density of states’. Consequently, it has been speculated that internal modes at high frequency (say above $\sim 1000\text{ cm}^{-1}$) and large momentum transfer values should be almost invisible with INS. However, this is largely in error. For example, CH stretching modes were observed at $\sim 3000\text{ cm}^{-1}$ and the role of the Debye–Waller factor had to be reconsidered.

It has been shown that the INS spectrum of potassium hydrogen carbonate (KHCO_3) cannot be represented with conventional harmonic force fields [62]. The observed intensities for lattice modes are smaller than calculated ones by at least one order of magnitude. There is virtually no riding effect. Protons are almost totally decoupled from the surrounding heavy atoms and their dynamics are better represented with localised modes in a ‘fixed’ (laboratory) referential frame. From the standpoint of the INS technique, KHCO_3 can be regarded as a crystal of protons so weakly coupled to the surrounding atoms that the framework of carbonate and potassium ions could be virtually ignored. Dynamical models are thus greatly simplified. Besides, this view is not specific to the ionic nature of the crystal. These results severely undermine the representation of vibrational spectra with usual normal modes. However, the phenomenological approach proposed so far lacks of contact with physics. It has been recently suggested that the peculiar proton dynamics could be a consequence of the non-local nature of quantum mechanics [63].

2.2. Proton transfer

Another highlight of the INS technique concerns proton transfer along pre-existing hydrogen bonds [47]. The prototypical KHCO_3 crystal contains centrosymmetric dimer entities $(\text{HCO}_3^-)_2$ and this structure remains unchanged from 298 to 14 K [64–66]. The hydrogen bond with length $\text{O}\cdots\text{O} = 2.59\text{ \AA}$ (2.61 \AA for KDCO_3) is moderately strong. At 298 K protons are disordered between two sites located at $\sim \pm 0.3\text{ \AA}$ off-centre of the hydrogen bond, with population ratio of $\sim 1:4$. However, diffraction studies cannot distinguish statistical and dynamical disorders.

The OH stretching vibration of KHCO_3 is of particular interest since quantum proton transfer (tunnelling) is best observed for vibrations along the reaction path. In the infrared and Raman, this mode gives broad bands, with several sub-maxima between 1800 and 3500 cm^{-1} [67–69]. Although various models have been proposed for hydrogen bond dynamics, and extensive quantum mechanical calculations have been performed [5,70], a detailed understanding of the band shaping mechanism is still lacking. In spite of these limitations, a quasi-symmetric double minimum potential along the proton-stretching mode coordinate was proposed (Fig. 1) [71]. The tunnelling transition associated with quantum transfer of a single proton was estimated at 213 cm^{-1} . Thanks to the great sensitivity of the INS technique to proton displacements with large amplitudes, this transition was observed at 216 cm^{-1} , close to the $\text{O}\cdots\text{O}$ stretching bands [62]. The dynamical nature of the proton disorder was thus established. If the potential were symmetrical, the tunnelling matrix element ν_{0t} corresponding to the splitting of the ground state would be equal to 18 cm^{-1} . The observed splitting of 216 cm^{-1} is largely due to the potential asymmetry.

Surprisingly, the tunnelling band is rather sharp. The measured full width at half maximum (FWHM) of $\sim 10\text{ cm}^{-1}$ is probably greater than the real bandwidth. This confirms that proton transfer is totally decoupled from heavy atom dynamics, in line with the remainder of the spectrum. Tunnelling transitions observed in various hydrogen bonds are quite similar [72–74]. These potentials correspond to the local transfer of a single proton. Clearly, the opportunity to observe tunnelling transitions with INS is an important step forward a better understanding of proton transfer dynamics. Further improvements of the spectrometer resolution should allow us to analyse tunnelling band shapes in more details.

3. Tautomerisation

A typical example of conflicting views arising from experiments carried out with different techniques is the tautomerisation mechanism in

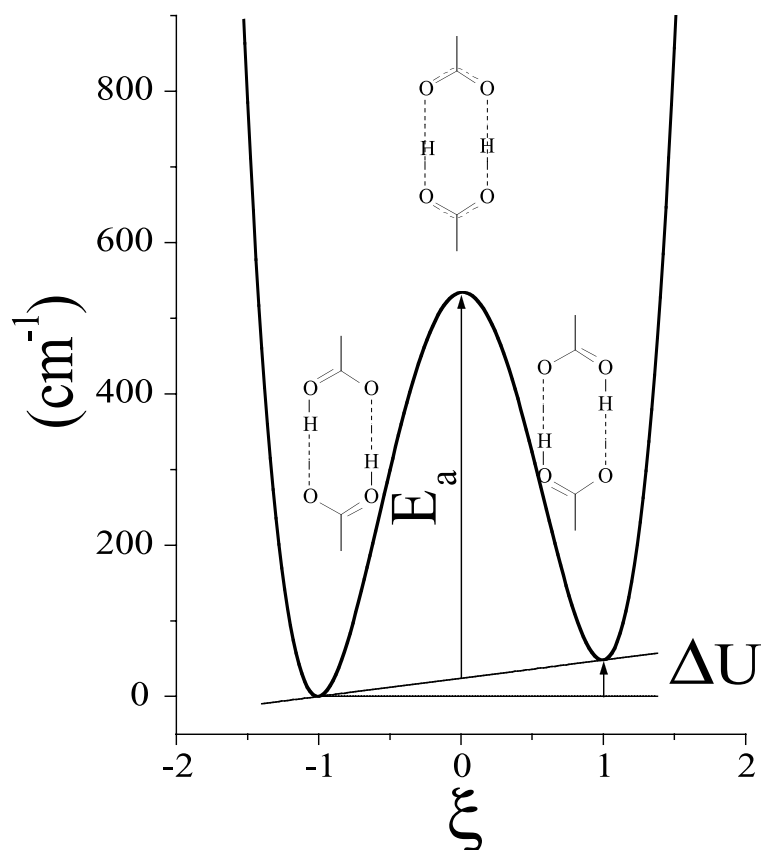
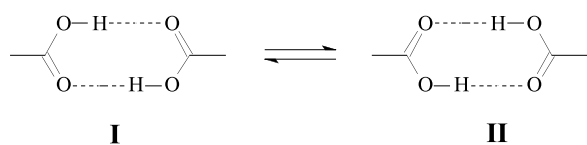


Fig. 2. Schematic view of the effective potential for concerted proton transfer in benzoic acid after Ref. [18]. The dimensionless reaction coordinate ξ is arbitrarily normalised.

centrosymmetric cyclic dimers of carboxylic acids:



For an isolated dimer **I** and **II** are equivalent and a symmetric double well potential is anticipated for simultaneous transfer of the two protons. In the crystalline state, intermolecular interaction may destroy the potential symmetry (Fig. 2).

The benzoic acid crystal (C_6H_5COOH) is largely regarded as a prototypical example of tautomerisation [11–14,16–32,75–98]. In the crystal, dimerisation takes place through hydrogen bonds across a centre of symmetry. The $O \cdots O$ distance of 2.608 Å at 20 K is slightly longer than in $KHCO_3$. The existence of

hydrogen atom disorder has been thoroughly investigated with NMR [13,14,16–30], QENS [14,21,31,32], vibrational spectroscopy [75–86], optical spectroscopy [87–94] and diffraction techniques [95–98].

Temperature effects observed for the $C=O$ stretching and OH bending bands in the infrared spectra of oriented crystals [75,77,78,82,86] were regarded as first evidences for the coexistence of tautomers **I** and **II** at thermal equilibrium. One component (at 1688 cm^{-1}) of the $\nu\text{ C=O}$ band whose intensity decreases at low temperature and almost disappears at $\sim 7\text{ K}$ was attributed to the less stable isomer (say **II**). A much weaker component at 1710 cm^{-1} that survives at low temperature was supposed to correspond to the most stable isomer **I**. The estimated energy difference was of $\sim 0.4\text{ kJ mol}^{-1}$ or $\sim 32\text{ cm}^{-1}$. For the OH bending modes, relative intensities are reversed. Strong bands at 1298,

1328 cm^{-1} (δ OH) and 948 cm^{-1} (γ OH) were attributed to the most stable configuration and much weaker bands at 1334 cm^{-1} (δ OH) and 959 cm^{-1} (γ OH) to the less stable isomer. Surprisingly, the OH stretching band profiles were ignored as if they were unaffected by tautomerisation. This is in marked contrast to the rather large frequency shifts reported for the CO stretching and OH bending modes.

Single-crystal neutron diffraction measurements provide unquestionable evidences for proton disorder [97,98]. The bridging protons are distributed over two sites separated by 0.70 Å at 20 K or 0.78 Å at 175 K. Simultaneously, the O...O distance increases from 2.608 to 2.629 Å and the relative population of the most stable form decreases from 0.87 (20 K), to 0.62 (175 K). The estimated energy difference between the two isomers is of $0.12 \pm 0.01 \text{ kcal mol}^{-1}$ or $40 \pm 3 \text{ cm}^{-1}$.

The tautomerisation rates derived from NMR T_1 relaxation [12,79–81] and QENS [14,21,31,32] measurements range from $\sim 10^8$ to 10^{11} s^{-1} as the temperature increases from liquid helium to room temperature. This is widely recognised as a case of transition from the quantum regime at low temperature (tunnelling) to the semi-classical regime at room temperature. These dynamics are represented with the Hamiltonian [12–15,17–22,27,32–35]:

$$H = H_\xi + H_{\xi Q} + H_Q. \quad (2)$$

The zero-order term H_ξ describes a pseudo-particle in a double well potential along the collective dimensionless coordinate ξ representing the simultaneous transfer of two protons (Fig. 2). The temperature dependence of the transfer rate is represented with coupling to a heat bath H_Q via $H_{\xi Q}$. In the phonon-assisted tunnelling model the coupling is normally limited to the bilinear term ($a\xi Q$) and the bath is represented with a set of harmonic oscillators [18].

In the usual representation of the tautomerism process not only the protons migrate simultaneously, as a rigid entity preserving the centre of symmetry, but also the skeleton is rearranged, as the electrons follow adiabatically the protons. Consequently, ξ is not simple. Potential surfaces calculated with quantum chemistry methods [9,12,15,27,30,32,33,41,43] and sophisticated analytical tools have been proposed to treat isolated non-rigid molecules [34–40,42]. However, calculations performed on isolated dimer entities

are not appropriate for $H_{\xi Q}$ and $H_{\xi Q}$. Moreover, it is difficult to model complex reaction paths in the crystalline state as long as combining advanced techniques of quantum chemistry with sophisticated analytical tools is not yet at the stage of being applied at the level of accuracy corresponding to vibrational spectroscopy.

For the practical purpose of data analysis the coordinate ξ is usually normalised in such a way that minima occur at arbitrarily chosen values ($\xi = \pm 1$, Fig. 2) and contributions from all atoms are included in the effective mass as a ‘mobility factor’. Estimated values of the mobility factor for benzoic acid between ~ 14 and 80 cm^{-1} [17,21,27] correspond to effective masses in the range from ~ 1 to 5 amu. With these approximations the detailed contribution of atom displacements to ξ is partially lost and it is not possible to distinguish reaction paths with the same effective mass. However, the Hamiltonian is simpler and the tautomerisation rate can be estimated analytically [18]:

$$\begin{aligned} \tau^{-1} = & \frac{3\pi}{2\hbar} a^2 \Delta U \left(\frac{\nu_{0r}}{\nu_D} \right)^2 \coth(\Delta U/2kT) \\ & + \tau_0^{-1} \{ \exp(-E_a/kT) \\ & + \exp[-(E_a - \Delta U)/kT] \}. \end{aligned} \quad (3)$$

At low temperature the quantum mechanism with negligible activation energy, referred to as ‘incoherent tunnelling’, determines the tautomerisation rate. The tunnelling matrix element ν_{0r} , the Debye frequency ν_D and the coupling strength a do not correspond to any observable quantities for NMR and QENS techniques. They have to be adjusted or, eventually, they can be transferred from other experimental or theoretical works [18]. The ‘coth’ term accounts for one-phonon emission/absorption due to coupling with the thermal bath. The second term in Eq. (3) represents the Arrhenius law for thermally activated barrier crossing. Eq. (3) has proven to be useful to interpret NMR and QENS data [11–15,17,19–33,99,100]. For benzoic acid, the estimated energy difference between **I** and **II** is $\Delta U = (58 \pm 1) \text{ cm}^{-1}$ [31] and the activation energy ranges from 400 to 500 cm^{-1} (1.2–1.5 kcal/mol) [12,21,30,32]. However, this equation does not fit well to the intermediate temperature range from liquid helium to room temperature and the best data

analysis with an increased number of adjustable parameters suggests three different dynamical regimes [31]. Qualitative explanation based on further tunnelling in excited vibrational states [29] and multiphonon relaxation [101] has been proposed. Quite recently, the concept of smooth transition between quantum mechanical and classical dynamics has been revisited [102].

4. Outstanding problems

Vibrational spectroscopy gives clear evidences that single proton transfer is a coherent quantum process along the quasi-linear stretching coordinate. The proton is virtually uncoupled to phonons and its effective oscillator mass is 1 amu. However, it is not yet demonstrated that these quantum dynamics can account for the interconversion rate up to room temperature on the much longer time-scales relevant to NMR and QENS.

The phonon-assisted tunnelling mechanism, eventually including additional terms that were ignored in the original theory, is successful to account for the tautomerisation rate at various temperatures. However, the resulting potential function is not appropriate for the quantum regime and largely inconsistent with vibrational spectroscopy. The conflicting views may arise from imperfection in modelling due to the lack of relevant information. In order to bridge the gap between dynamical models, it is necessary to collect information with all experimental techniques.

The benzoic acid crystal is the best candidate for this purpose. It has been thoroughly investigated with many techniques of interest for proton transfer studies, except temperature effects with Raman. However, the previous interpretation of the infrared spectra in terms of thermal equilibrium between two isomers [77,78] is not satisfactory. For example, diffraction measurements or quantum chemistry calculation [86] reveal that the two isomers are identical and cannot be distinguished. Therefore, to attribute the C=O stretching modes at 1688 and 1710 cm^{-1} to different isomers with different absorption coefficients [77,78,82,86] is questionable. Furthermore, a detailed analysis of the spectral profiles of the broad ν OH bands between 2500 and 3000 cm^{-1} , analogous to those previously performed for KHCO_3

and KDCO_3 [71], should provide information on the potential function for single proton transfer. So far these bands were totally ignored [77]. Therefore, we have undertaken systematic studies of the infrared and Raman spectra of various isotopic derivatives of the benzoic acid crystal. In this report, the double minimum potential function for proton transfer is totally determined from experimental data.

5. Experimental

The fully hydrogenated (BA- h_6) and ring deuterated (BA- d_5h) benzoic acids were commercial products. They were sublimated. The OD derivative BA- h_5d was obtained after three exchanges with commercial methanol CH_3OD .

5.1. Crystal structure and symmetry

At room temperature, the benzoic acid crystal is monoclinic, $P2_1/c$ (C_{2h}^5) with four molecules in the unit cell [95–98]. There are 177 vibrational modes that can be decomposed into 156 internal and 21 external vibrations. In the present work, the benzene vibrations are largely ignored, in as much as they do not interfere with the bridging protons. [76]. The external modes can be represented as 12 hydrogen bond vibrations ($3A_g + 3B_u + 3A_u + 3B_g$), six Raman active lattice vibrations corresponding to librations of dimers around the three axes of inertia ($3A_g + 3B_g$) and three infrared active translational vibrations of one dimer with respect to the other ($2A_u + B_u$). In the (a, b) plane, the A_u or B_u modes are extinguished for electrical field vectors parallel to the a or b crystal axes, respectively [85].

5.2. Spectra

Infrared spectra were recorded with a FTIR Perkin Elmer[®] 983 with a mean resolution of $\sim 2 \text{ cm}^{-1}$. Powdered samples in Nujol[®] or Fluorolube[®] mulls between KBr plates were loaded into a closed cycle refrigerator. It is difficult to estimate the effective temperature of the sample from that measured with a thermometer on the plates. Fortunately, the intensity at a maximum of the very sharp band at 1787 cm^{-1} (BA- h_6) is very sensitive to temperature (see below)

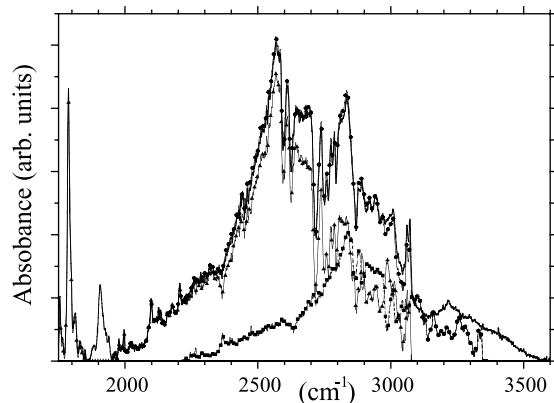


Fig. 3. Infrared spectrum of the fully hydrogenated benzoic acid at 16 K in the OH stretching region. Powdered sample. Tentative self-consistent decomposition into two components.

and visual comparison with the spectra presented in Ref. [77] confirms that effective temperatures of the samples were similar in all experiments. Spectra are free of saturation effects.

The Raman spectra were obtained with an RTI-DILOR[®] triple monochromators equipped with an Ar⁺ laser. Powdered samples were sealed in capillary glass tubes and then loaded into a liquid helium cryostat. The temperature was measured with a thermometer just above the sample.

The INS spectrum of BA-*d*₅*h* is the same as that presented in Refs. [103,104]. The original file (TRSL3033.ana) was downloaded from the TFXA database at the ISIS pulsed neutron source (Ruther-

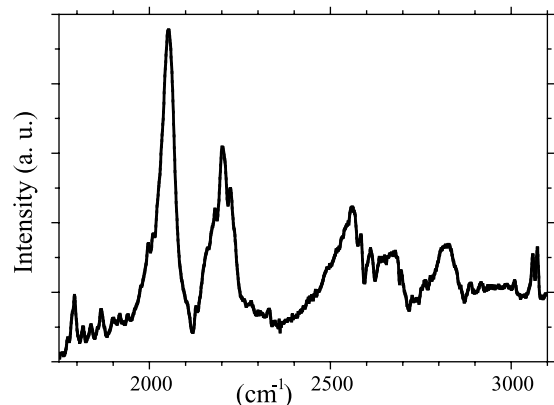


Fig. 4. Infrared spectra of an isotope mixture of the fully hydrogenated benzoic acid (~5%) and OD (BA-*h*₅*d* ~95%) analogue at 15 K. Powdered sample.

ford Appleton Laboratory, Chilton, Didcot, Oxon, UK).

5.3. Calculations

Energy levels and wave functions were calculated with the variational method [105–108] utilising a basis sets of 40 harmonic wave functions with fundamental frequency $\hbar\omega_0$. For each potential function, the parameter ω_0 is optimised so as to obtain the lowest energy for the ground state. The transition moment of order n for transition $i \rightarrow j$ is calculated according to $M_{ij}^n = \int \Psi_i x^n \Psi_j dx$.

6. The OH and OD stretching modes

A full analysis of the vibrational spectra of benzoic acid and partially deuterated analogues is beyond the scope of this paper. The discussion is focussed on the OH/OD stretching band profiles in the infrared.

The ν OH and ν OD bands are very weak in Raman. They are largely hidden by the extremely intense ν CH or ν CD bands at ~ 3000 and 2300 cm^{-1} , respectively, and cannot be distinguished from overtones and combinations in the same spectral range. These bands are not discussed any further.

In the infrared, the ν OH and ν OD profiles are complex (Figs. 3 and 4). The ν OH mean frequency is little affected by ring deuteration and temperature effects below ~ 150 K.

The doublets at $1787\text{--}1906 \text{ cm}^{-1}$ for BA-*h*₆ ($1788\text{--}1902 \text{ cm}^{-1}$ for BA-*d*₅*h*) show spectacular temperature effects. The components are ill defined at room temperature. They become sharp and intense at low temperature without any significant frequency shift. Frequencies are close to those anticipated for the ν OH or ν CH overtones but the corresponding intensities should be very weak and temperature effects are not those anticipated for Fermi resonance with the main ν OH band. These sharp doublets are attributed to ‘zero-phonon’ transitions (see below) [109–112], analogous to those observed for KHCO₃ [71].

Several band shaping mechanisms associated to hydrogen bond formation contribute to the spectral profiles [109–126]: mechanical and electrical anharmonicity, strong coupling with hydrogen bond modes,

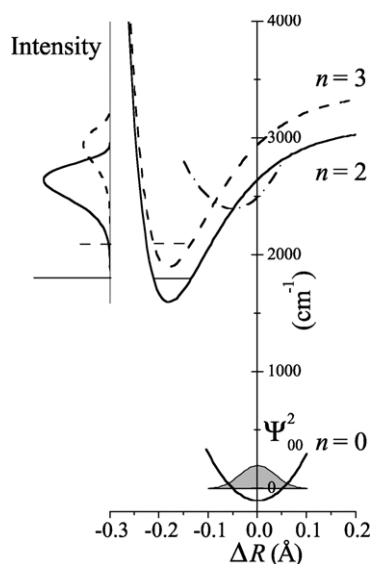


Fig. 5. Schematic representation of the adiabatic potentials for the slow ν O...O mode (ΔR coordinate) in the states $n = 2$ (solid) and $n = 3$ (dash) of the ν OH mode. The broad profiles are determined by the density probability $\Psi_0^2(\Delta R)$ in the ground state. The sharp zero-phonon bands are transitions to the stationary ground states in the upper potentials. The profiles obtained for the zero-order dipole derivative $d\mu/dR = 0$ are shown. The dot dash curve is a tentative representation of an adiabatic potential for a phonon.

Fermi resonance, interaction of the broad ν OH profile with sharp overtones or combinations of skeleton modes (Evans transmission windows [127]), dynamical correlation (Davydov coupling), tunnel splitting, etc. It is not easy to unravel these contributions.

Davydov coupling can be eliminated safely because dynamical correlation between OH oscillators are cancelled in an isotopic mixture containing $\sim 95\%$ BA- h_{5d} and $\sim 5\%$ BA- h_6 (Fig. 4). The sample contains $\sim 90\%$ of fully deuterated dimers, less than 1% of totally hydrogenated dimers and $\sim 9\%$ of mixed dimers. The residual ν OH profile is thus largely due to mixed dimers free of H...H dynamical coupling. Apart from intensity, the ν OH profile is very similar to that observed for the fully hydrogenated crystal. The main maxima of intensity at 2570 and 2840 cm^{-1} remain at the same frequency. Therefore, Davydov coupling between protons is negligible. This is in marked contrast to the large intradimer coupling of the ν C=O modes.

The ν OD profile is composed of two well-resolved components at 2050 and 2205 cm^{-1} . Temperature

effects on intensities and frequencies are tiny. The full widths at half maximum (FWHM) are 44 and 58 cm^{-1} , respectively, and the intensity ratio I_{2050}/I_{2205} is of $\sim 1.4 \pm 0.1$. This ratio is not compatible with a Fermi resonance between the overtone of the ν OD mode at $\sim 1000 \text{ cm}^{-1}$ and the ν OD mode. (The intensity of the overtone should be weaker than or similar to that of the fundamental).

As dynamical coupling is eliminated it is possible to correlate the ν OH profile with the ν OD bands. For BA- h_6 at 16 K the maxima of intensity at 2570 and 2840 cm^{-1} can be regarded as the analogues of the ν OD bands at 2050 and 2205 cm^{-1} , respectively. Then, the ν OH profile can be decomposed into two virtually identical broad components with an intensity ratio $I_{2560}/I_{2820} \sim 2.0 \pm 0.1$. The splitting is $\sim 270 \text{ cm}^{-1}$ and the FWHM of each component is $\sim 250 \text{ cm}^{-1}$. In addition, to each component we associate one of the sharp bands at 1786 and 1906 cm^{-1} , respectively. The two profiles are very similar but the splitting is not rigorously a constant over the whole spectral range. It increases from $\sim 120 \text{ cm}^{-1}$ below 2000 cm^{-1} to $\sim 270 \text{ cm}^{-1}$ at $\sim 3000 \text{ cm}^{-1}$. The frequency ratio ν OH/ ν OD for the main components (2570/2050 ~ 1.25 and 2840/2205 ~ 1.29) and the spectacular narrowing of the profiles upon deuteration confirm strong anharmonicity. Similar band decomposition was performed for BA- d_5h .

The decomposition of the ν OH bands into two similar broad profiles cannot be explained with conventional Fermi resonance. For example, Fermi resonance with overtones of the δ OH containing modes between 1250 and 1350 cm^{-1} should occur in a limited spectral range, roughly between 2500 and 2700 cm^{-1} . Such a local effect cannot account for the band splitting extending itself from 1700 to 3000 cm^{-1} .

The profile for each component is similar to those previously reported for various hydrogen bonds with O...O distances of $\sim 2.6 \text{ \AA}$ [62,71,111,112]. The shape arises from strong anharmonic coupling with the O...O modes due to the fast decrease of the ν OH frequency with the length of the hydrogen bond [109, 110,112,114,116,117,123–125]. Within the framework of adiabatic separation of the fast ν OH and slow ν O...O modes the upper adiabatic potential for the ν O...O mode $V_i(\Delta R)$ can be represented as a Morse-like potential whose minimum is shifted toward short

O··O distances with respect to the equilibrium position in the ground state (Fig. 5) [109,118,128]. Owing to the huge coupling the excited state is largely aperiodic and the dynamics can be treated within the short-time approximation [118]. The spectral density $I(\nu)$ at $\nu = V_i(\Delta R)$ is proportional to the probability density for the slow coordinate ΔR and to the derivative of the dipole moment: $I[\nu = V_i(\Delta R)] \propto \Psi_0^2(\Delta R) d\mu/d\Delta R$ [118]. The narrow peaks at low frequency (between 1750 and 2000 cm^{-1}) are zero-phonon transitions from the ground state to the lowest state of the upper potential. This state can have rather long lifetime at low temperature because near the minimum of the upper potential $d\nu/d\Delta R \sim 0$ and the strong coupling is cancelled. As opposed to ν OH, the ν OD frequency decreases much less rapidly with the length of the hydrogen bond [117]. The anharmonic coupling is weaker and the ν OD bands are narrower.

In principle, the shapes of the upper potentials can be adjusted in order to obtain the best fit to the spectral profile [111,112]. However, it is difficult to account for the fine structure superimposed to the broad profiles. Additional coupling with other modes must be included. Apart from the ν O··O, phonon modes are only weakly coupled to ν OH. The adiabatic potentials along the ΔR coordinate for combinations of these modes with the ν OH transition should be identical to the Morse-like function for the ν OH mode itself. They should give a manifold of broad profiles, practically indistinguishable. As opposed to that the observed fine structure demonstrates that adiabatic potentials for phonons have also well-defined minima along ΔR , presumably shifted with respect to the equilibrium position in the ground state (one of these adiabatic curves is artistically represented as a dot dash curve in Fig. 5). The observed spectral profiles are likely due to a manifold of interaction and possibly avoided crossing among all these adiabatic potentials.

Regarding the large number of unknown parameters, a more quantitative analysis in terms of multidimensional coupling with lattice modes [114, 116,121–126] is beyond the scope of this paper. The conclusion of importance to the remainder of this work is that the main splitting of the ν OH and ν OD bands can be attributed to proton tunnelling in a double minimum potential (see Section 7). Fermi

resonance, combination and dynamical correlation are only marginal band shaping mechanisms.

7. Proton transfer dynamics

In this section, the two components of the ν OH and ν OD bands are attributed to the $0 \rightarrow 2$ and $0 \rightarrow 3$ transitions within asymmetrical double minimum potentials similar to those previously proposed for KHCO_3 and KDClO_3 [71]. This assignment scheme deserves consideration as alternative band shaping mechanisms (dynamical correlation, Fermi resonance, etc. discussed above) have been eliminated. The potential function for the proton-stretching mode can be written as:

$$V(x) = ax + bx^2 + c \exp(-dx^2). \quad (4)$$

The coordinate x represents the H or D position along the O··O bond. The contribution of the C=O coordinates to the effective coordinate for proton transfer is ignored and the effective oscillator mass is that of a bare H or D atom. The parameters a , b , c and d can be determined from experimental values: ν_{02} and ν_{03} for the $0 \rightarrow 2$ and $0 \rightarrow 3$ transitions, the distance between the two minima R and the intensity ratio I_{03}/I_{02} .

Unfortunately, some ambiguities cannot be avoided. First, ν_{02} and ν_{03} depend on which part of the ν OH profile is considered. For BA- h_6 , $\nu_{02} = 2570 \text{ cm}^{-1}$ and $\nu_{03} = 2840 \text{ cm}^{-1}$ correspond to a maximum of probability. Second, the intensity ratio depends on the unknown electrical anharmonicity. Third, the distance between the two proton sites of $\sim 0.70 \text{ \AA}$, derived from diffraction data at 20 K [97, 98] corresponds to the distance between maxima of the probability density. This is a good approximation to the distance between the potential minima only if x is parallel to the O··O direction. Otherwise, if the reaction path were significantly bent, the effective distance between potential minima along the curvilinear coordinate could be longer.

The observation of the ν_{01} transition is a necessary confirmation of the double minimum potential. This transition is anticipated in a frequency range below $\nu_{03} - \nu_{02} = 270 \text{ cm}^{-1}$ and most probably around 200 cm^{-1} [71]. The intensity should be extremely

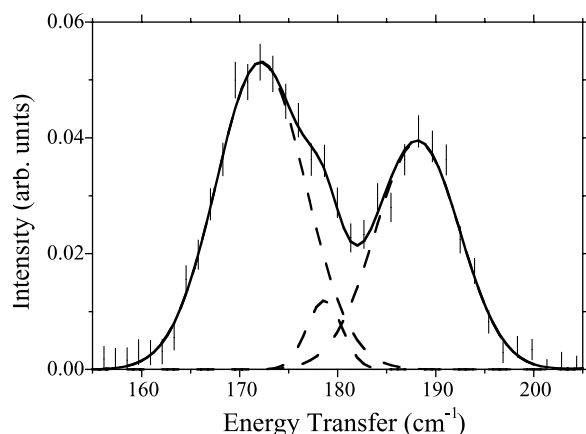


Fig. 6. Inelastic neutron scattering spectrum of the ring deuterated derivative BA- d_5h at 20 K [103,104]. Experimental (error bars), band decomposition into three Gaussian components (dash line) and best fit (solid line).

weak in the infrared or Raman and the band should be difficult to distinguish among other contributions in the same frequency range. The INS spectrum of BA- d_5h offers the best opportunity to observe this transition because the scattering cross-section for H atoms is very much greater than for D, C or O atoms and this technique has great sensitivity to proton displacements with large amplitudes.

In the original work [104], only two INS bands at 172 and 189 cm^{-1} were distinguished in the range from 130 to 250 cm^{-1} . However, the INS profile between 150 and 210 cm^{-1} is better decomposed into three bands at 172, 178 and 188 cm^{-1} (Fig. 6). The weak band at 178 cm^{-1} is the antisymmetric τ_a COO mode observed in the infrared ($A_u + B_u$) [85]. The band at 188 cm^{-1} is the symmetric τ_s COO mode observed at 189 cm^{-1} in Raman ($A_g + B_g$). This assignment scheme is in accordance with the observed intensities, as the mean square amplitudes for proton displacements and the INS intensities are much smaller for the antisymmetric than for the symmetric modes. The band at 172 cm^{-1} previously attributed to the τ_a COO mode is re-attributed to ν_{01} . This band has no visible counterpart in the infrared or Raman. It is rather narrow (FWHM $\sim 10 \text{ cm}^{-1}$) and cannot be confused with the broad density of states for the lattice modes below 150 cm^{-1} . To assign this band to the τ_a COO mode [104] would be in conflict with the

infrared, INS and Raman spectra. Unfortunately, ab initio calculations are not very helpful as they give a rather broad frequency range from ~ 140 to 187 cm^{-1} for the τ COO modes [104].

The potential function presented in Fig. 7 gives the best fits to the observed transitions. The calculated intensity ratio for the first order term of the transition moment ($I_{2560}/I_{2820} = 2.8$) is compatible with the observed ratio of ~ 2 and modest electrical anharmonicity. Frequencies calculated for the OD stretching with the same potentials correspond to the bands observed at 2050 and 2205 cm^{-1} (Fig. 4) to within $\sim 4\%$ accuracy. However, the calculated intensity ratio $I_{(2050)}/I_{(2205)} \sim 500$ is quite different from the observed ratio of ~ 1.5 . It would be unreasonable to attribute such a great difference to a dramatic change of the dipole moment derivative upon deuteration. Presumably, there is a significant decrease of the potential barrier in the deuterated sample, as previously reported for KDCO_3 , compared to KHCO_3 [71].

The INS intensity of the $0 \rightarrow 1$ transition depends strongly on the delocalisation degree of the wave functions, which can be estimated by numerical integration. About 2% of the wave function is delocalised and the observed INS intensity for the $0 \rightarrow 1$ transition is depressed by a factor $\epsilon^2 \sim 3 \times 10^{-4}$, compared to the symmetrical double minimum potential. Nevertheless, owing to the great sensitivity of INS and to the high performances of the spectrometer this band is observed with reasonable signal to noise ratio (Fig. 6).

The narrow $0 \rightarrow 1$ transition is in marked contrast to the broad ν OH profiles for the $0 \rightarrow 2$ and $0 \rightarrow 3$ transitions whose widths are related to the fast variation of the frequencies ν_{02} and ν_{03} with the O...O distance ($\sim 12,000 \text{ cm}^{-1} \text{ \AA}^{-1}$ [117]). In comparison to that the variation of ν_{01} with the O...O distance is determined by the potential asymmetry ($[dV/dx]_{x=0} = 265 \text{ cm}^{-1} \text{ \AA}^{-1}$) and the band broadening due to this coupling is negligible.

The distance of 0.7 Å between the two minima of the potential presented in Fig. 7 is very similar to the distance between the two proton sites given by neutron diffraction [97,98]. Therefore, the reaction path for proton transfer is along the straight line between the two sites. If the effective mass for proton transfer was significantly greater than 1 amu, the

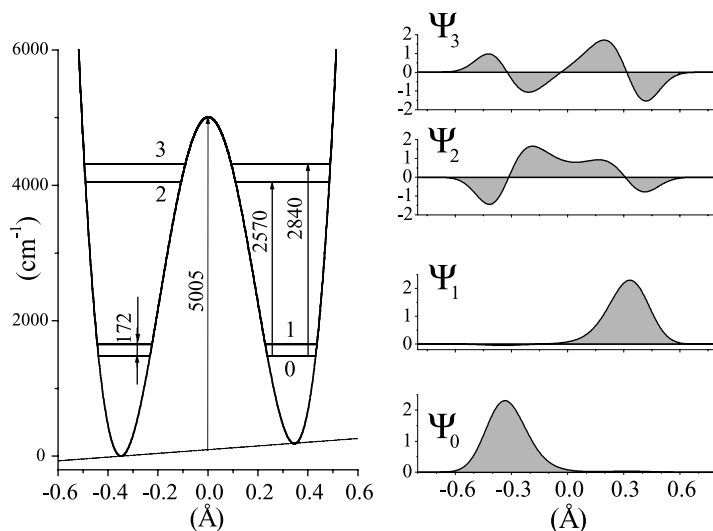


Fig. 7. Potential function (left) and wave functions (right) for the proton-stretching mode of benzoic acid. $V(x) = 266x + 286,000x^2 + 171,480 \exp(-2.165x^2)$. V and x are in cm^{-1} and Å units, respectively. The particle mass is 1 amu.

distance between the minima of the potential accounting for the same energy levels should be even smaller. It can be firmly concluded that the effective mass is 1 amu within experimental errors and coupling with heavy atoms is negligible.

As mentioned above, the infrared spectra do not allow us to define uniquely ν_{02} and ν_{03} . Different values would give slightly different values for the barrier height. However, within the two state model approximation [18] this would be of very little consequences for the lower states and the for proton dynamics at any temperature.

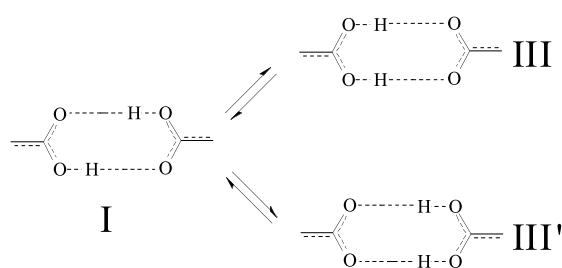
The great similarity of the potential functions for the ν OH modes in KHCO_3 and benzoic acid suggests that the potential is specific to the strength of the $\text{OH}\cdots\text{O}$ hydrogen bond with only marginal perturbation by hydrogen-bonded entities (CO_3^{2-} ions or molecular entities in benzoic acid) and crystal field. This is in line with the correlation between the OH stretching frequency and the $\text{O}\cdots\text{O}$ distance [117].

8. Interconversion dynamics

The potential function for the ν OH mode derived from the infrared spectra is the effective potential resulting from averaging the multidimensional poten-

tial, as a function of all degrees of freedom for the system, over the range of the hyper surface spanned by the other degrees of freedom. In quantum mechanics, the potential function is an operator for which only eigen states are relevant whereas trajectories are undefined. The effective potential operator that determines the spectral profile corresponds to a minimum of the total energy of the system with respect to all degrees of freedom except the stretching coordinate. This is the quantum analogue to the classical reaction path for proton transfer that is a geodesic of the hyper surface. The effective potential operator depends on the zero-point energy of the whole system. A change of the potential barrier upon deuteration is a consequence of the restricted domain spanned by the other degrees of freedom compared to the hydrogenated analogue. The effective potential for the deuterated system is closer to the potential function along the geodesic corresponding to the classical trajectory. Indeed, for an infinite mass the classical and quantum mechanical dynamics should be identical.

From the viewpoint of chemistry, the lowest potential minimum in Fig. 7 corresponds to **I** and the other minimum corresponds to isomers **III** or **III'** in which one of the protons is transferred along the hydrogen bond.



For each state ($n = 0$ or 1) the probabilities $P_n(\mathbf{I})$, $P_n(\mathbf{III})$ and $P_n(\mathbf{III}')$ are defined as the squared wave functions integrated over the corresponding domains. For example, $P_0(\mathbf{I}) = \int_{\mathbf{I}} dx \Psi_0^2(x) \sim 1$ and $P_0(\mathbf{III}) = P_0(\mathbf{III}') = \int_{\mathbf{III}} dx \Psi_0^2(x) = \epsilon^2$. Therefore, the states $n = 0$ and 1 are virtually, but not exactly, pure species \mathbf{I}_0 and \mathbf{III}_1 (\mathbf{III}'_1), respectively. In the upper states ($n = 2, 3, \dots$) the wave functions are largely delocalised and isomers are no longer distinguishable.

The spectra at low temperature correspond to \mathbf{I}_0 . At room temperature the relative populations of the $n = 0$ and 1 states are similar and isomers \mathbf{III}_1 and \mathbf{III}'_1 should be visible. As there is no significant effect in the COO stretching region, it can be concluded that proton transfer occurs without significant structural change of the COO groups. The double minimum function is the effective potential due to the mean crystal field for a mean geometry of the carboxylic groups. This is quite different from the tautomerism mechanism in which electrons are supposed to follow adiabatically the motions of protons [80]. At the present stage of investigation, there is apparently no consistency between the potential functions presented in Figs. 2 and 7. Isomers \mathbf{III}_1 and \mathbf{III}'_1 do not correspond to the intermediate structure at the saddle point in Fig. 2. To the least, the barrier of $\sim 500 \text{ cm}^{-1}$ is certainly unrealistic for proton transfer as it is much lower than the zero-point energy of the proton modes. In the quantum regime, this barrier is irrelevant.

9. Conclusion

The vibrational spectra obtained with complementary techniques (infrared, Raman and INS) reveal new dynamics for protons engaged in hydrogen bonds in crystals.

In KHCO_3 the proton dynamics are largely decoupled from the lattice. At the present stage of investigation, the physical origin of this decoupling is not clear. Among many possible factors, anharmonicity, crystal field symmetry and quantum effects should play an important role.

The double minimum potentials for the transfer of a single proton along the hydrogen bond are very similar for KHCO_3 and benzoic acid. The $0 \rightarrow 1$ transitions are clearly observed with INS. The potential barriers of $\sim 5000 \text{ cm}^{-1}$ impose that the transfer occurs exclusively via tunnelling and semi-classical jumps over the barrier are irrelevant. The proton transfer dynamics in the centrosymmetric dimers are uncorrelated. Proton transfer occurs without any visible rearrangement of the carboxylic group structure and the effective proton mass is close to 1 amu. The adiabatic approximation where electrons follow the slow proton motions is not adequate. Further experimental and theoretical investigation should contribute to a more consistent representation of the interconversion dynamics in various systems.

References

- [1] G.C. Pimentel, A.L. McClellan, *The Hydrogen Bond*, Freeman, San Francisco, 1960.
- [2] L. Pauling, *The Nature of the Chemical Bond*, Cornell University Press, Ithaca, NY, 1960.
- [3] S.N. Vinogradov, R.H. Linnell, *Hydrogen Bonding*, Van Nostrand-Reinhold, New York, 1971.
- [4] M.D. Joesten, L.J. Schaad, *Hydrogen Bonding*, Marcel Dekker, New York, 1974.
- [5] P. Schuster, G. Zundel, C. Sandorfy, *The Hydrogen Bond: Recent Developments in Theory and Experiments*, North-Holland, Amsterdam, NY, 1976.
- [6] P. Schuster, *Hydrogen Bonds*, Springer, Berlin, 1984.
- [7] G.A. Jeffrey, W. Saenger, *Hydrogen Bonding in Biological Structures*, Springer, Berlin, 1991.
- [8] S. Scheiner, *Hydrogen Bonding: A Theoretical Perspective*, Oxford University Press, Oxford, 1997.
- [9] M.E. Tuckerman, D. Marx, M.L. Klein, M. Parinello, *Science* 275 (1997) 817.
- [10] C.L. Perrin, J.B. Nielson, *Annu. Rev. Phys. Chem.* 48 (1997) 511.
- [11] R. Graf, R. Meyer, T.-K. Ha, R.R. Ernst, *J. Chem. Phys.* 75 (1981) 2914.
- [12] B.H. Meier, F. Graf, R.R. Ernst, *J. Chem. Phys.* 76 (1982) 767.
- [13] A. Gough, M.M.I. Haq, J.A.S. Smith, *Chem. Phys. Lett.* 117 (1985) 389.

- [14] A. Stöckli, A. Furrer, C. Schoenenberger, B.H. Meier, R.R. Ernst, I. Anderson, *Phys. B* 136 (1986) 161.
- [15] S. Benz, U. Haebleren, *J. Magn. Res.* 66 (1986) 125.
- [16] T. Agaki, F. Imashiro, T. Terao, N. Hirota, S. Hayashi, *Chem. Phys. Lett.* 139 (1987) 331.
- [17] R. Meyer, R.R. Ernst, *J. Chem. Phys.* 86 (1987) 784.
- [18] J.L. Skinner, H.P. Trommsdorff, *J. Chem. Phys.* 89 (1988) 897.
- [19] A.J. Horsewill, A. Aibout, *J. Phys.: Condens. Matter* 1 (1989) 9609.
- [20] R. Meyer, R.R. Ernst, *J. Chem. Phys.* 93 (1990) 5518.
- [21] A. Stöckli, B.H. Meier, R. Meyer, R.R. Ernst, *J. Chem. Phys.* 93 (1990) 1502.
- [22] A. Heuer, U. Haebleren, *J. Chem. Phys.* 95 (1991) 4201.
- [23] S. Takeda, A. Tsuzumitani, C.A. Chatzidimitriou-Dreismann, *Chem. Phys. Lett.* 198 (1992) 316.
- [24] A.J. Horsewill, A. Heidemann, S. Hayashi, *Z. Phys. B* 90 (1993) 319.
- [25] A.J. Horsewill, P.J. McDonald, D. Vijayaraghavan, *J. Chem. Phys.* 100 (1994) 1889.
- [26] A.J. Horsewill, A. Ikram, I.B.I. Tomsah, *Mol. Phys.* 84 (1995) 1257.
- [27] C. Scheurer, P. Saalfrank, *Chem. Phys. Lett.* 245 (1995) 201.
- [28] D.F. Brougham, A.J. Horsewill, A. Ikram, R.M. Ibberson, P.J. McDonald, M. Pinter-Krainer, *J. Chem. Phys.* 105 (1996) 979.
- [29] D.F. Brougham, A.J. Horsewill, R.I. Jenkinson, *Chem. Phys. Lett.* 272 (1997) 69.
- [30] A.J. Horsewill, D.F. Brougham, R.I. Jenkinson, C.J. McGloin, H.P. Trommsdorff, M.R. Johnson, *Ber. Bunsenges. Phys. Chem.* 102 (1998) 317.
- [31] M. Neumann, D.F. Brougham, C.J. McGloin, M.R. Johnson, A.J. Horsewill, H.P. Trommsdorff, *J. Chem. Phys.* 109 (1998) 7300.
- [32] M.A. Neumann, S. Cracium, A. Corval, M.R. Johnson, A.J. Horsewill, V.A. Benderskii, H.P. Trommsdorff, *Ber. Bunsenges. Phys. Chem.* 102 (1998) 325.
- [33] V.P. Sakun, M.V. Vener, N.D. Sokolov, *J. Chem. Phys.* 105 (1996) 379.
- [34] V.A. Benderskii, E.V. Vetoshkin, S.Y. Grebenshchikov, L.v. Laue, H.P. Trommsdorff, *Chem. Phys.* 219 (1997) 119.
- [35] V.A. Benderskii, E.V. Vetoshkin, L.v. Laue, H.P. Trommsdorff, *Chem. Phys.* 219 (1997) 143.
- [36] V.A. Benderskii, E.V. Vetoshkin, H.P. Trommsdorff, *Chem. Phys.* 244 (1999) 273.
- [37] V.A. Benderskii, E.V. Vetoshkin, H.P. Trommsdorff, *Chem. Phys.* 244 (1999) 299.
- [38] V.A. Benderskii, E.V. Vetoshkin, *Chem. Phys.* 257 (2000) 203.
- [39] V.A. Benderskii, I.S. Irgibaeva, E.V. Vetoshkin, H.P. Trommsdorff, *Chem. Phys.* 262 (2000) 369.
- [40] V.A. Benderskii, E.V. Vetoshkin, I.S. Irgibaeva, H.P. Trommsdorff, *Chem. Phys.* 262 (2000) 393.
- [41] V. Barone, C. Adamo, *J. Chem. Phys.* 105 (1996) 11007.
- [42] W. Siebrand, Z. Smerdarchina, M.Z. Zgierski, A. Fernandez-Ramos, *Int. Rev. Phys. Chem.* 18 (1999) 5.
- [43] M.E. Tuckerman, D. Marx, *Phys. Rev. Lett.* 86 (2001) 4946.
- [44] M. Ichikawa, *Chem. Phys. Lett.* 79 (1981) 583.
- [45] P. Gilli, V. Bertolasi, V. Ferretti, G. Gilli, *J. Am. Chem. Soc.* 116 (1994) 909.
- [46] B.H. Meier, R. Meyer, R.R. Ernst, P. Zolliker, A. Furrer, W. Hälg, *Chem. Phys. Lett.* 103 (1983) 169.
- [47] G.J. Kearley, F. Fillaux, M.-H. Baron, S.M. Bennington, J. Tomkinson, *Science* 264 (1994) 1285.
- [48] J.E. DelBene, M.J.T. Jordan, *Int. Rev. Phys. Chem.* 18 (1999) 119.
- [49] S.W. Lovesey, *Nuclear Scattering, Theory of Neutron Scattered from Condensed Matter*, vol. I, Clarendon, Oxford, 1984.
- [50] E.B. Wilson Jr., J.C. Decius, P.C. Cross, *Molecular Vibrations*, McGraw-Hill, New York, 1955.
- [51] P. Barchewitz, *Spectroscopie Infrarouge*, Gauthier-Villars, Paris, 1967.
- [52] S.J. Cyvin, *Molecular Vibrations and Mean-Square Amplitudes*, Elsevier, Amsterdam, 1968.
- [53] A.I. Kitaigorodsky, *Molecular Crystals and Molecules*, Academic Press, New York, 1973.
- [54] S. Califano, V. Schettino, N. Neto, *Lattice Dynamics of Molecular Crystals*, Springer, Berlin, 1981.
- [55] A.J. Pertsin, A.I. Kitaigorodsky, *The Atom-Atom Potential Method*, Springer Series in Chemical Physics, Springer, Berlin, 1987.
- [56] A.C. Zemach, R.J. Glauber, *Phys. Rev.* 101 (1956) 118.
- [57] H. Jobic, J. Tomkinson, A. Renouprez, *Mol. Phys.* 39 (1980) 989.
- [58] H. Jobic, R.E. Gosh, A. Renouprez, *J. Chem. Phys.* 75 (1981) 4025.
- [59] A. Griffin, H. Jobic, *J. Chem. Phys.* 75 (1981) 5940.
- [60] G.J. Kearley, *J. Chem. Soc. Faraday Trans. II* 82 (1986) 41.
- [61] H. Jobic, H. Lauter, *J. Chem. Phys.* 88 (1988) 5450.
- [62] F. Fillaux, J. Tomkinson, J. Penfold, *Chem. Phys.* 124 (1988) 425.
- [63] F. Fillaux, *Phys. D* 113 (1998) 172.
- [64] J.O. Thomas, R. Tellegren, I. Olovsson, *Acta Cryst. B* 30 (1974) 1155.
- [65] J.O. Thomas, R. Tellegren, I. Olovsson, *Acta Cryst. B* 30 (1974) 2540.
- [66] A. Cousson, Unpublished.
- [67] A. Novak, P. Saumagne, L.D.C. Bock, *J. Chim. Phys. Phys.-Chim. Biol.* 60 (1963) 1385.
- [68] K. Nakamoto, Y.A. Sarma, K. Ogoshi, *J. Chem. Phys.* 43 (1965) 1177.
- [69] G. Lucazeau, A. Novak, *J. Raman Spectrosc.* 1 (1973) 573.
- [70] H. Ratajczak, W.J. Orville-Thomas, *Molecular Interactions*, vol. 1, Wiley, New York, 1980.
- [71] F. Fillaux, *Chem. Phys.* 74 (1983) 405.
- [72] F. Fillaux, A. Lautié, J. Tomkinson, G.J. Kearley, *Chem. Phys.* 154 (1991) 135.
- [73] F. Fillaux, J. Tomkinson, *Chem. Phys.* 158 (1991) 113.
- [74] F. Fillaux, J. Tomkinson, *J. Mol. Struct.* 270 (1992) 339.
- [75] S. Hayashi, N. Kimura, *Bull. Inst. Chem. Res. Kyoto Univ.* 44 (1955) 335.
- [76] L. Colombo, K. Furic, *Spectrochim. Acta* 27A (1971) 1773.
- [77] S. Hayashi, J. Umemura, *J. Chem. Phys.* 60 (1974) 2630.

- [78] S. Hayashi, J. Umemura, *J. Chem. Phys.* 63 (1975) 1732.
- [79] S. Nagaoka, T. Terao, F. Imashiro, A. Saika, N. Hirota, S. Hayashi, *Chem. Phys. Lett.* 80 (1981) 580.
- [80] S. Nagaoka, N. Hirota, T. Matsushita, K. Nishimoto, *Chem. Phys. Lett.* 92 (1982) 498.
- [81] S. Nagaoka, T. Terao, F. Imashiro, A. Saika, N. Hirota, S. Hayashi, *J. Chem. Phys.* 79 (1983) 4694.
- [82] S. Hayashi, J. Umemura, S. Kato, K. Morokuma, *J. Phys. Chem.* 88 (1984) 1330.
- [83] R. Nakamura, K. Machida, S. Hayashi, *J. Mol. Struct.* 146 (1986) 101.
- [84] R. Nakamura, K. Machida, M. Oobatake, S. Hayashi, *Mol. Phys.* 64 (1988) 215.
- [85] H.R. Zelsmann, Z. Mielke, *Chem. Phys. Lett.* 186 (1991) 501.
- [86] S. Hayashi, M. Oobatake, R. Nakamura, K. Machida, *J. Chem. Phys.* 94 (1991) 4446.
- [87] J.M. Clemens, R.M. Hochstrasser, H.P. Trommsdorff, *J. Chem. Phys.* 80 (1984) 1744.
- [88] G.R. Holtom, R.M. Hochstrasser, H.P. Trommsdorff, *Chem. Phys. Lett.* 131 (1986) 44.
- [89] R.M. Hochstrasser, H.P. Trommsdorff, *Chem. Phys.* 115 (1987) 1.
- [90] H.P. Trommsdorff, *J. Lumin.* 38 (1987) 129.
- [91] H.P. Trommsdorff, R.M. Hochstrasser, M. Pierre, *J. Lumin.* 40 and 41 (1988) 203.
- [92] A. Oppenländer, C. Rambaud, H.P. Trommsdorff, *J.C. Vial, Phys. Rev. Lett.* 63 (1989) 1432.
- [93] C. Rambaud, A. Oppenländer, M. Pierre, H.P. Trommsdorff, *J.C. Vial, Chem. Phys.* 136 (1989) 335.
- [94] C. Rambaud, A. Oppenländer, H.P. Trommsdorff, *J.C. Vial, J. Lumin.* 45 (1990) 310.
- [95] G.A. Sim, J.M. Robertson, T.H. Goodwin, *Acta Cryst.* 8 (1955) 157.
- [96] R. Feld, M.S. Lehmann, K.W. Muir, J.C. Speakman, *Z. Kristallogr.* 157 (1981) 215.
- [97] C.C. Wilson, N. Shankland, A.J. Florence, *Chem. Phys. Lett.* 253 (1996) 103.
- [98] C.C. Wilson, N. Shankland, A.J. Florence, *J. Chem. Soc., Faraday Trans.* 92 (1996) 5051–5057.
- [99] A.J. Horsewill, A. Aibout, *J. Phys.: Condens. Matter* 1 (1989) 9609.
- [100] B.H. Meier, F. Graf, R.R. Ernst, *J. Chem. Phys.* 76 (1982) 767.
- [101] R. Silbey, H.P. Trommsdorff, *Chem. Phys. Lett.* 165 (1990) 540.
- [102] L. Latanowicz, E.C. Reynhardt, *Chem. Phys. Lett.* 341 (2001) 561.
- [103] H.P. Trommsdorff, M.R. Johnson, M. Neumann, L. vonLaue, D.F. Brougham, A.J. Horsewill, NATO ASI Series, Kluwer Academic Publishers, Dordrecht, 1997, p. 369A.
- [104] M. Plazanet, N. Fukushima, M.R. Johnson, A.J. Horsewill, H.P. Trommsdorff, *J. Chem. Phys.* 115 (2001) 3241.
- [105] E. Heilbronner, H. Rutishauser, F. Gerson, *Helv. Chim. Acta* 42 (1959) 2304.
- [106] E. Heilbronner, H. Rutishauser, F. Gerson, *Helv. Chim. Acta* 42 (1959) 2285.
- [107] R.L. Somorjai, D.F. Hornig, *J. Chem. Phys.* 36 (1962) 1980.
- [108] T.R. Singh, J.L. Wood, *J. Chem. Phys.* 48 (1968) 4567.
- [109] S. Fischer, G.L. Hofacker, M.A. Ratner, *J. Chem. Phys.* 52 (1970) 1934.
- [110] G. Hofacker, Y. Maréchal, M. Ratner, in: P. Schuster, G. Zundel, C. Sandorfy (Eds.), *The Hydrogen Bond/I Theory*, vol. I, North-Holland, Amsterdam, 1976, p. 297.
- [111] F. Fillaux, B. Marchon, A. Novak, *Chem. Phys.* 86 (1984) 127.
- [112] L. Soulard, F. Fillaux, *Chem. Phys.* 100 (1985) 355.
- [113] B.I. Stepanov, *Nature* 157 (1946) 808.
- [114] Y. Maréchal, A. Witkowski, *J. Chem. Phys.* 48 (1968) 3697.
- [115] Y. Maréchal, *Chem. Phys. Lett.* 13 (1972) 237.
- [116] A. Witkowski, M. Wojcik, *Chem. Phys.* 1 (1973) 9.
- [117] A. Novak, *Struct. Bonding Berlin* 18 (1974) 177.
- [118] F. Fillaux, *Chem. Phys.* 74 (1983) 395.
- [119] Y. Maréchal, *Chem. Phys.* 79 (1983) 69.
- [120] Y. Maréchal, *Chem. Phys.* 79 (1983) 85.
- [121] Y. Maréchal, *Vibrational Spectra and Structure*, Elsevier, Amsterdam, 1987.
- [122] Y. Maréchal, *J. Chem. Phys.* 87 (1987) 6344.
- [123] D. Chamma, O. Henri-Rousseau, *Chem. Phys.* 248 (1999) 53.
- [124] D. Chamma, O. Henri-Rousseau, *Chem. Phys.* 248 (1999) 71.
- [125] D. Chamma, O. Henri-Rousseau, *Chem. Phys.* 248 (1999) 91.
- [126] P. Blaise, O. Henri-Rousseau, *Chem. Phys.* 256 (2000) 85.
- [127] J.C. Evans, *Spectrochim. Acta* 18 (1962) 507.
- [128] N.D. Sokolov, V.A. Savel'ev, *Chem. Phys.* 22 (1977) 383.